



Generation of a near-circularly-polarized pulse from a ring-current state of a Ne atom in an orthogonally polarized two-color laser field

Yun-He Xing , Jun Zhang, Xiao-Xin Huo, Lin Sun, Shuang Wang, Zi-An Li, and Xue-Shen Liu*
Institute of Atomic and Molecular Physics, Jilin University, Changchun 130012, China

 (Received 30 August 2023; revised 19 December 2023; accepted 5 January 2024; published 25 January 2024)

We investigate theoretically the elliptically high-order harmonic generation from the ring-current state of the Ne atom by numerically solving the two-dimensional time-dependent Schrödinger equation in an orthogonally polarized two-color (OTC) laser fields. We find that the elliptically polarized harmonics can be generated by the ring-current state with nonzero angular momentum. A high-efficiency near-circularly-polarized single-atom radiation pulse can be obtained by adjusting the intensity ratio of the OTC laser fields. As the intensity ratio increases, the efficiency of the harmonics is enhanced and the ellipticity of the harmonics is increased, which is illustrated by the temporal evolution of the electronic density probability and the semiclassical three-step model. Moreover, we find that the ellipticity of a single-atom radiation pulse is sensitive to the relative phase of the OTC laser fields, which offers the possibility to control the polarization of extreme ultraviolet radiation.

DOI: [10.1103/PhysRevA.109.013111](https://doi.org/10.1103/PhysRevA.109.013111)

I. INTRODUCTION

High-order harmonic generation (HHG) is a highly nonlinear process in strong laser-matter interactions. The dynamics of HHG can be understood by the three-step-recollision model, i.e., ionization, acceleration, and recombination [1]. A high-order harmonic spectrum contains abundant information about structures and dynamics for target matters, which is widely used for ultrafast detection, including atoms [2–4], molecules [5,6], and solids [7–9]. In addition, HHG is one of the main sources to obtain tabletop extreme ultraviolet or soft-x-ray attosecond pulses [10,11], which have important applications in research areas such as physics, chemistry, and biology. Therefore, HHG has been a hot topic of research. In recent years, circularly polarized isolated attosecond pulses (IAPs) and attosecond pulse trains (APT) have received a great deal of attention. Compared to linearly polarized attosecond pulses, they offer additional degrees of freedom and have important applications in chiral recognition [12–14], the study of ultrafast chiral-specific dynamics [15], and magnetic circular dichroism spectroscopy [16,17].

To date, various schemes for generating elliptical polarized attosecond pulses have been proposed. The simplest scheme to obtain high-order harmonics with nonzero ellipticity is that using an elliptically polarized laser field, but the efficiency of the harmonics decreases as the ellipticity increases for the driving laser field [18,19]. The other option is based on using prealigned molecules [20–22], and in this case the ellipticity of the high-order harmonics is not very high. To improve the efficiency and ellipticity of the harmonics, one of the effective methods is to use the bichromatic counterrotating circularly polarized (BCCP) driving laser fields [23,24]. Pure circularly polarized harmonics can be produced under this

electric field and the efficiency is comparable to that of a linearly polarized driving field. However, due to the selection rule [25,26], the high harmonic spectrum consists of alternating double peaks with left and right circular polarization. The ellipticity of the synthesized attosecond pulses is obviously limited due to the opposite harmonic helicity. Huang *et al.* [27] overcame this problem by adjusting the ellipticity of the BCCP laser pulse, achieved the adjustment of the polarization state of the attosecond pulse, and obtained the attosecond pulse with large ellipticity. In addition, Gensheim and Rost [28] proposed to obtain elliptically polarized high harmonics from twisted electron wave packets with quantized orbital angular momentum along the laser polarization axis driven by a linearly polarized field.

Recently, the elliptically polarized IAPs and APTs from the ring-current state have attracted attention [29–31]. Although the single atom does not emit attosecond pulses when interacting with the laser field, there is a natural attosecond timescale that characterizes harmonic generation processes based on the numerical solution of the time-dependent Schrödinger equation (TDSE) in microscopic laser-atom interactions as discussed in Ref. [32]. The process that leads to attosecond extreme ultraviolet (XUV) emission begins at the single-atom level when an electron in the bound state encounters a laser field of sufficient strength to cause ionization [32]. By numerically solving the TDSE, we can analyze the XUV radiation on the attosecond timescale at the microscopic level, while to generate an attosecond pulse in experiment we need to further consider the macroscopic propagation effects.

The ring-current state has been demonstrated through extensive theoretical and experimental work. For example, ring currents can be induced from neon and benzene [33], excited atoms using circularly polarized pulse [34], and selected ionization in ions [35]. The single ring-current state can be excited in a suitable molecule or atom by a circularly polarized π pulse [34,36], i.e., the $2p_+$ and $2p_-$ ring-current states of

*liuxs@jlu.edu.cn

the Ne atom can be induced by a clockwise or a counterclockwise rotating circularly polarized π pulse, respectively. The single ring-current state as a research target has been used in previous works [29,30,37].

Neufeld and Cohen [33] demonstrated the elliptically polarized high harmonics from the ring-current state by symmetry breaking; they indicated that if the medium carries a ring current, the symmetry-based selection rule will be broken, which will cause the emission of elliptically polarized harmonics. It was demonstrated that elliptically polarized harmonics can be obtained from the ring-current states. However, in practical applications, the improvement of the efficiency and the ellipticity of the attosecond pulse is a key issue. Therefore, an effective scheme to generate a near-circularly-polarized attosecond pulse with high efficiency is still desired.

In this paper we present a scheme for generating a near-circularly-polarized single-atom radiation pulse with high efficiency from the ring-current state of the Ne atom, which is based on the orthogonally polarized two-color (OTC) laser fields. By adjusting the intensity ratio of the OTC laser fields, both the efficiency and the ellipticity of the harmonics can be improved. A near-circularly-polarized single-atom radiation pulse can be obtained at a certain field strength ratio or by adjusting the relative phase of the OTC laser fields. We investigate the temporal evolution of the probability density of the electron wave packet and the classical electron trajectory, which is used to illustrate the physical mechanism of the harmonic emission. Our results provide potential tools to explore molecular chiral structures and manipulate magnetic materials.

II. THEORETICAL METHODS

In this work we investigate the elliptically high-order harmonic generation from the ring-current state of the Ne atom by numerically solving the two-dimensional (2D) time-dependent Schrödinger equation (unless stated otherwise, atomic units are used throughout this paper)

$$i \frac{\partial \psi(\mathbf{r}, t)}{\partial t} = H(\mathbf{r}, t) \psi(\mathbf{r}, t), \quad (1)$$

where $H(\mathbf{r}, t) = -\frac{1}{2} \nabla^2 + V(\mathbf{r}) + \mathbf{r} \cdot \mathbf{E}(t)$ is the full Hamiltonian and $\mathbf{r} = (x, y)$ indicates the position of the electron in the 2D x - y plane, with $V(\mathbf{r})$ the 2D model Coulomb potential of the Ne atom, which is taken from [29]

$$V(\mathbf{r}) = -\frac{Z(\mathbf{r})}{\sqrt{r^2 + a}}, \quad (2)$$

where $Z(\mathbf{r}) = 1 + 9 \exp(-r^2)$. The soft-core parameter a is set to 2.881 72 to obtain the ionization potential 0.793, which is the same as the first ionization potential of the Ne atom [38]. The ring-current state of the Ne atom with magnetic quantum numbers $m = \pm 1$ can be expressed as $|\varphi_{2p_{\pm}}\rangle = 1/\sqrt{2}(|\varphi_{2p_x}\rangle \pm i|\varphi_{2p_y}\rangle)$ [29–31]. The $|\varphi_{2p_x}\rangle$ and $|\varphi_{2p_y}\rangle$ are obtained by imaginary-time propagation filtering out the ground-state wave function [29,39]; $|\varphi_{2p_x}\rangle$ and $|\varphi_{2p_y}\rangle$ are degenerate states with the same ionization potential 0.793. For a reference atom calculation, we use the $1s$ orbital as the initial state and take $Z(\mathbf{r}) = 1$ and $a = 0.1195$ to keep the same ionization potential for the $2p$ orbital of the Ne atom as

used in Ref. [29]. The $1s$ state with zero angular momentum can be compared with the nonzero angular momentum $2p_+$ state, which reflects the influence of angular momentum in the harmonic emission process.

The external electric field is an OTC laser pulse

$$\mathbf{E}(t) = E_0 f(t) [\sin(\omega_0 t) \bar{e}_x + \gamma \sin(2\omega_0 t + \phi) \bar{e}_y], \quad (3)$$

where E_0 and ω_0 are the maximum amplitudes of the pulse and frequency of the fundamental field, respectively; $f(t)$ is a trapezoidal envelope of the laser pulse with a total duration of three optical cycles (o.c.) with one cycle of rise and fall; γ is the intensity ratio, which can reflect the relative amplitude of the two laser fields; ϕ is the relative phase; and \bar{e}_x and \bar{e}_y are the unit vectors in the x and y directions, respectively. We numerically solve the 2D TDSE by using the split-operator method to obtain the propagation of the time-dependent wave function $\psi(\mathbf{r}, t)$. We use a grid of size 409.6 a.u. containing 2048 grid points on the x (y) axis. The space and time steps are 0.4 and 0.05 a.u., respectively. The HHG spectrum is obtained from the absolute square of the Fourier transformation of the time-dependent dipole acceleration

$$P_r(\omega) = \left| \int \exp(-i\omega t) a_r(t) dt \right|^2. \quad (4)$$

The time-dependent dipole acceleration can be expressed as

$$a_r(t) = \langle \psi(\mathbf{r}, t) | -\partial H(\mathbf{r}) / \partial \mathbf{r} | \psi(\mathbf{r}, t) \rangle. \quad (5)$$

The dipole acceleration in the frequency domain can be calculated from $d_{x,y}(\Omega) = \int a_{x,y}(t) e^{-i\Omega t} dt$. The harmonic radiation can be divided into left (d_-) and right (d_+) rotation polarized components, which can be obtained by $d_{\pm} = (d_x \pm id_y) / \sqrt{2}$. The ellipticity of the harmonics can be obtained from

$$\varepsilon = \frac{|d_+| - |d_-|}{|d_+| + |d_-|}. \quad (6)$$

The harmonic spectrum can be projected into two counter-rotating components: the right circularly polarized (RCP) harmonics $P_+ = |d_+|^2$ and the left circularly polarized (LCP) harmonics $P_- = |d_-|^2$ [40]. The temporal profile of the single-atom radiation pulse can be obtained by superimposing several harmonics, and the dependence of the intensity on time can be expressed as

$$I_{x,y}(t) = \left| \sum_q a_{x,y}(q) e^{iq\omega t} \right|^2, \quad (7)$$

where $a_{x,y}(q) = \int a_{x,y}(t) e^{-iq\omega t} dt$ and q is the harmonic order [41].

III. RESULTS AND DISCUSSION

Figure 1(a i) shows the RCP and LCP harmonic components from the ring-current state $2p_+$ with nonzero angular momentum of the Ne atom driven by the OTC laser fields. The two-dimensional Lissajous projection of the OTC laser fields is shown in the inset of Fig. 1(a ii). Here we choose $E_0 = 0.075 49$ a.u. ($I_0 = 2 \times 10^{14}$ W/cm²), $\omega_0 = 0.057$ a.u. (800 nm), $\phi = 0$, and the intensity ratio of the OTC laser

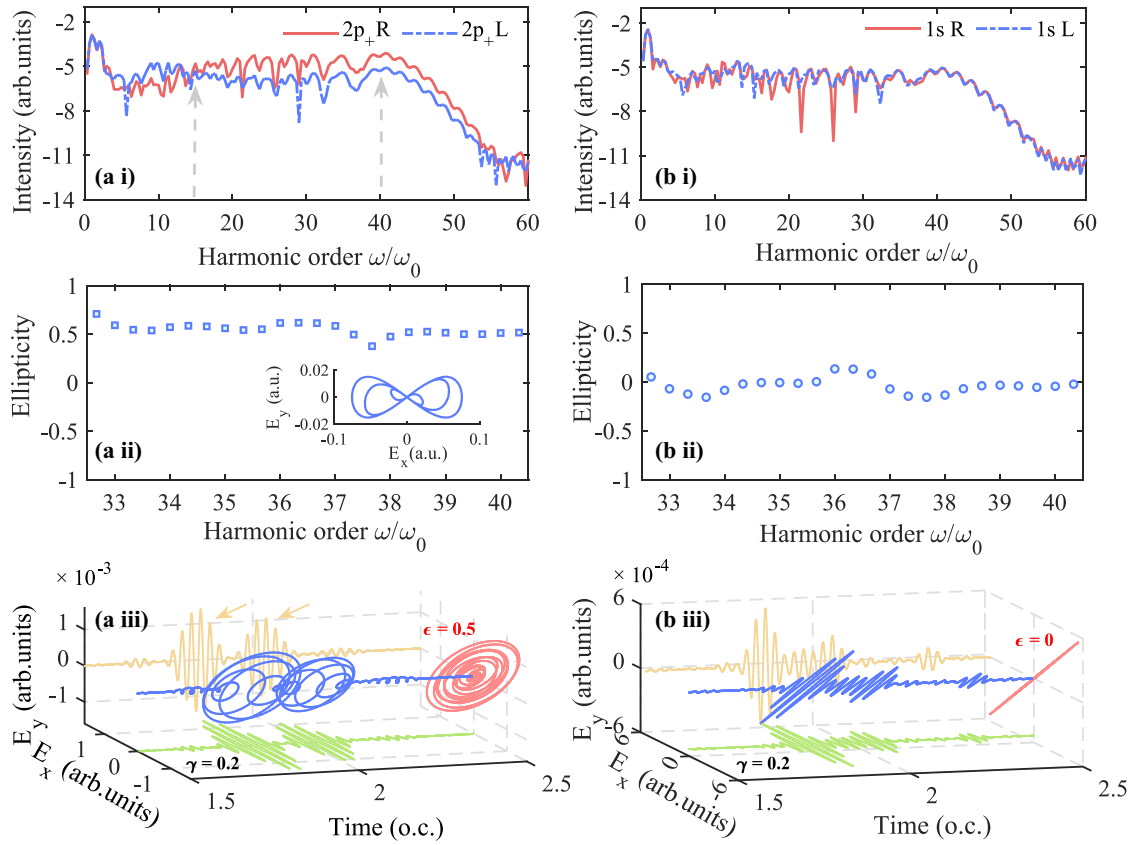


FIG. 1. (a i) and (b i) Harmonic spectrum of the RCP and LCP components driven by the OTC laser fields. (a ii) and (b ii) Ellipticity of the harmonics near the cutoff region (33rd to 40th order). (a iii) and (b iii) Three-dimensional plot of the electric field of the single-atom radiation pulse by superimposing the 33rd- to 40th-order harmonics. (a) is from the ring-current state $2p_+$ of the Ne atom and (b) is from the $1s$ orbital of the reference atom. The fundamental laser intensity is 2×10^{14} W/cm² and the wavelength is 800 nm. The relative phase is $\phi = 0$ and the intensity ratio is $\gamma = 0.2$. The inset of (a ii) is the two-dimensional Lissajous projection of the OTC laser fields. The harmonic intensity is on a logarithmic scale.

fields $\gamma = 0.2$. In our scheme, the pulse with elliptical polarization is generated by selecting the target atoms rather than by adjusting the BCCP laser fields, which is the main difference from Ref. [27]. From Fig. 1(a i) we can see that the intensity of the RCP and LCP harmonic components are significantly different. In the plateau region (14th order to 40th order, as indicated by the gray arrows) the intensity of the RCP component is higher than that of the LCP component, which indicates that the harmonics emitted are right-rotation polarized.

In Figs. 1(a ii) and 1(a iii) we present the ellipticity of the harmonics near the cutoff position (from 33rd to 40th order) and the 3D electric field of the single-atom radiation pulse by superimposing these harmonics [32]. We can see that the ellipticity of the harmonic shown in Fig. 1(a ii) is close to 0.5. From Fig. 1(a iii) we can see that the radiation is a pulse train with ellipticity 0.5, which has two intensity peaks (yellow arrows) in one optical cycle.

For comparison we present the RCP and LCP harmonics from the $1s$ state of the reference atom in Fig. 1(b i). We can see that the RCP and LCP harmonics have the same intensity, which indicates that the harmonics are linearly polarized. It is the fact that OTC laser fields are composed of linearly polarized lasers in the x and y directions and that atoms are isotropic symmetric systems, which leads to linearly polarized

harmonic emission. Similarly, in Figs. 1(b ii) and 1(b iii) we show the ellipticity of the harmonics near the cutoff position (from 33rd to 40th order) and the 3D electric field of the radiation by superimposing these harmonics. We can see that the ellipticity of the harmonics is almost zero and the radiation is linearly polarized.

By comparing the ellipticity of the high-order harmonics from different initial states, we can see that the ring-current state has an important effect on the polarization of harmonic emission. The ring-current state has nonzero angular momentum, and during the recombination process, the angular momentum of the electron in the ring-current state can be transferred to the polarization state of the emitted photons. Thus, the harmonic from the ring-current state is elliptically polarized, which is consistent with previous reports and can be demonstrated by a simple derivation of the equation [29,30]. This process can also be understood from another perspective, i.e., the ring-current state carries angular momentum and this symmetry-based selection rule is broken, causing the emission of elliptically polarized harmonics [33]. However, in our results for $\gamma = 0.2$ the intensity and ellipticity of the single-atom radiation pulse are low. The ellipticity of the radiation pulse is only 0.5, which is not an ideal result. Next we investigate the effect of the intensity ratio γ on the ellipticity and emission efficiency of the high-order harmonics from the

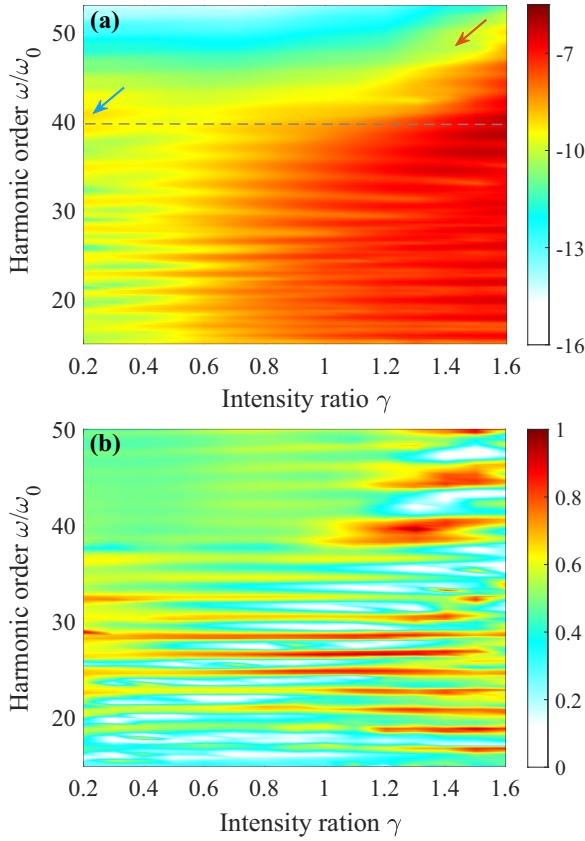


FIG. 2. (a) Intensity and (b) ellipticity distribution of the harmonics versus harmonic order and intensity ratio. The blue arrow and the red arrow indicate the cutoff position of the harmonics around 40th for $\gamma = 0.2$ and 50th for $\gamma = 1.4$, respectively. The dashed line indicates the reference value for the 40th harmonic. The initial state is the ring-current state $2p_+$ of the Ne atom. The other laser parameters are the same as those in Fig. 1. The harmonic intensity is on a logarithmic scale.

ring-current state. Figures 2(a) and 2(b) show the intensity and ellipticity distributions of the harmonics as a function of the intensity ratio γ and the harmonic order (the intensity ratio γ is from 0.2 to 1.6). From Fig. 2(a) we can see that the harmonic intensity gradually increases as γ increases, with the strongest harmonic intensity around $\gamma = 1.4$. In addition, as γ increases the cutoff position of the harmonics is extended [as indicated by red arrow in Fig. 2(a)]. From Fig. 2(b) we can see that the ellipticity of the harmonics increases as the intensity ratio γ increases. Similarly, around $\gamma = 1.4$ the ellipticity reaches a maximum. Note that by controlling the intensity ratio γ the two ideal conditions are simultaneously met, i.e., the harmonic emission efficiency is enhanced and the harmonic ellipticity is increased.

We demonstrate the single-atom radiation pulse by superimposing the 29th- to 39th-order harmonics near the cutoff position for the intensity ratio $\gamma = 1.3$ and the 31st- to 42nd-order harmonics for $\gamma = 1.4$. To reflect the polarization characteristic of the pulse, we present the 3D plot of the electric field of the pulse as shown in Figs. 3(a i) and 3(b i), respectively. Figures 3(a ii) and 3(b ii) show the projection of the electric field of the pulse onto the E_x - E_y plane. From

Fig. 3(a ii) we can see that the ellipticity of the radiation pulse is 0.8 and is right-rotation polarized (red arrow) for $\gamma = 1.3$. From Fig. 3(b ii) we can see that the ellipticity of the radiation pulse is 0.98 for $\gamma = 1.4$. The electric field is also right-rotation polarized and the ellipticity is close to 1, which means that the radiation pulse is near-circularly polarized. Figures 3(a iii) and 3(b iii) present the time-dependent intensity of the radiation pulse. We can see that the radiation pulse with durations of 239 and 293 as can be obtained for $\gamma = 1.3$ and 1.4, respectively. The above results show that near-circularly-polarized single-atom radiation pulse with high efficiency can be obtained by adjusting the intensity ratio of the OTC laser fields.

Next we illustrate the physical mechanism of a high-efficiency near-circularly-polarized single-atom radiation pulse from quantum and classical perspectives, respectively. In Fig. 4 we present the temporal evolution of the probability density of the electron wave packets for the intensity ratios $\gamma = 0.2$ and 1.4, which can reflect the motion of the electrons visually. We show the temporal evolution of the electronic probability density from $T = 1.5$ to 1.9 o.c. with an interval of 0.1 o.c. Figures 4(a) and 4(b) show the results for $\gamma = 0.2$ and 1.4, respectively. From Fig. 4(a) we can see that the electron moves mainly from the $-x$ axis direction to the $+x$ axis direction and has a small helical trajectory. It returns to the parent nucleus at the moments around $T = 1.8$ and 1.9 o.c., as shown in Figs. 4(a iv) and 4(a v) (white arrows). In the case of $\gamma = 0.2$, the electric-field intensity in the x direction is $E_x = 0.07549$ ($I_x = 2 \times 10^{14}$ W/cm²) and in the y direction it is $E_y = 0.01509$ ($I_y = 8 \times 10^{12}$ W/cm²). The electric-field strength in the y direction is very weak compared to that in the x direction; it has little effect on the electron motion. Thus, the electron motion has a small helical trajectory for $\gamma = 0.2$, which is similar to the probability density of the electron wave packet from the ring-current state driven by the linearly polarized laser field as demonstrated in Fig. 1(c) of Ref. [30]. From Figs. 4(b i)–4(b iv) we can see that the electron moves with a larger helical trajectory for $\gamma = 1.4$, moving about twice as far as that for the $\gamma = 0.2$ case. Similarly, at the moments $T = 1.8$ and 1.9 o.c., the electron returns to the parent nucleus as shown in Figs. 4(b iv) and 4(b v) (white arrows). For the case of $\gamma = 1.4$, the electric-field intensity in the x direction is $E_x = 0.07549$ ($I_x = 2 \times 10^{14}$ W/cm²) and in the y direction it is $E_y = 0.10568$ ($I_y = 3.9 \times 10^{14}$ W/cm²). Due to the enhancement of the electric-field strength in the y direction, the electrons have large helical trajectory.

By comparing the temporal evolution of the electron probability density for $\gamma = 0.2$ and 1.4 (wave functions for $\gamma = 0.2$ and 1.4 have been normalized), we find that the electron density for $\gamma = 1.4$ is about two orders of magnitude larger than that for $\gamma = 0.2$. The position of the nucleus is at the origin of the coordinates. The electron wave packets for $\gamma = 0.2$ [see Figs. 4(a iv) and 4(a v)] and $\gamma = 1.4$ [see Figs. 4(b iv) and 4(b v)] return to the nucleus at about $T = 1.8$ and 1.9 o.c. The above analysis indicates that more electrons can return to the nucleus for $\gamma = 1.4$ than that for $\gamma = 0.2$; thus the harmonic intensity for $\gamma = 1.4$ is higher, which is consistent with the result demonstrated in Fig. 2(a).

Neufeld and Cohen [33] indicated that the ring-current state carries angular momentum, which will break the sym-

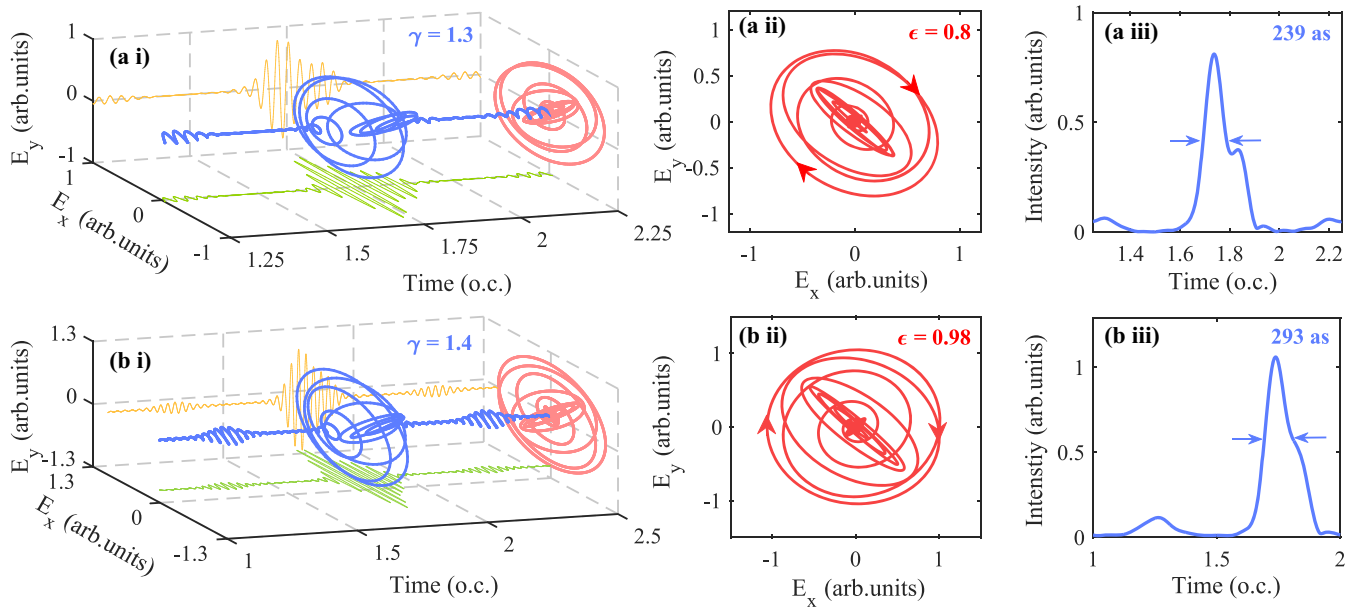


FIG. 3. Three-dimensional plot of the electric field of the near-circularly-polarized single-atom radiation pulse by superimposing the (a i) 29th- to 39th-order harmonics for $\gamma = 1.3$ and (b i) 31st- to 42nd-order harmonics for $\gamma = 1.4$. The electric field of the radiation pulse is projected into the E_x - E_y plane for (a ii) $\gamma = 1.3$ and $\epsilon = 0.8$ and (b ii) $\gamma = 1.4$ and $\epsilon = 0.98$. The time-dependent intensity of the radiation pulse is shown for the cases of (a iii) $\gamma = 1.3$ and 239 as and (b iii) $\gamma = 1.4$ and 293 as. The initial state is the $2p_+$ state and the other laser parameters are the same as those in Fig. 1.

metry of the system. The angular momentum deflects the ionized electrons away from the x axis, so the intensity of the y component of the harmonics is not zero. It is also shown that the harmonics from ring-current state driven by the OTC laser fields will have larger ellipticity due to the fact that the electrons have a helical trajectory in OTC laser fields. The intensity of the y component of the harmonics will increase, which makes the intensity of the x and y components of the harmonics close to each other, and therefore the ellipticity of the harmonics is larger. For the case of $\gamma = 0.2$, the electrons are less distributed in the y axis direction and move mainly in the x direction with a small helical trajectory returning to

the nucleus [see Figs. 4(a iv) and 4(a v)]. However, for the case of $\gamma = 1.4$, the helical trajectory of the electron wave packet is larger and more electrons return to the nucleus along the y axis [see Figs. 4(b iv) and 4(b v)], which enhances the intensity of the y component of the harmonics; this means that the intensity of the x and y components of the harmonics will be closer together. This satisfies the condition for generating harmonics with large ellipticity, i.e., the intensity of the x and y components of the harmonics should be the same [42]. Therefore, the harmonics have larger ellipticity in the case of $\gamma = 1.4$. Our result is consistent with that described in Ref. [33]. In addition, the electron moves farther, which

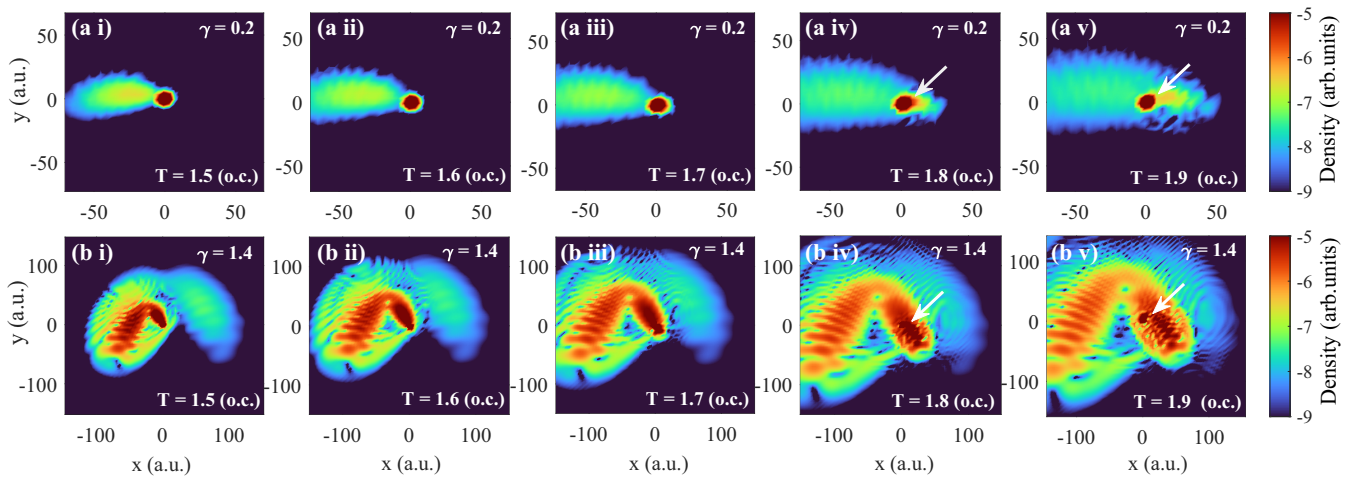


FIG. 4. Temporal evolutions of the probability density of the electron wave packets for the intensity ratio (a) $\gamma = 0.2$ and (b) $\gamma = 1.4$. The wave functions for $\gamma = 0.2$ and $\gamma = 1.4$ have been normalized. The coordinate zero point indicates the position of the nucleus. The initial state is the $2p_+$ state and the other laser parameters are the same as those in Fig. 1.

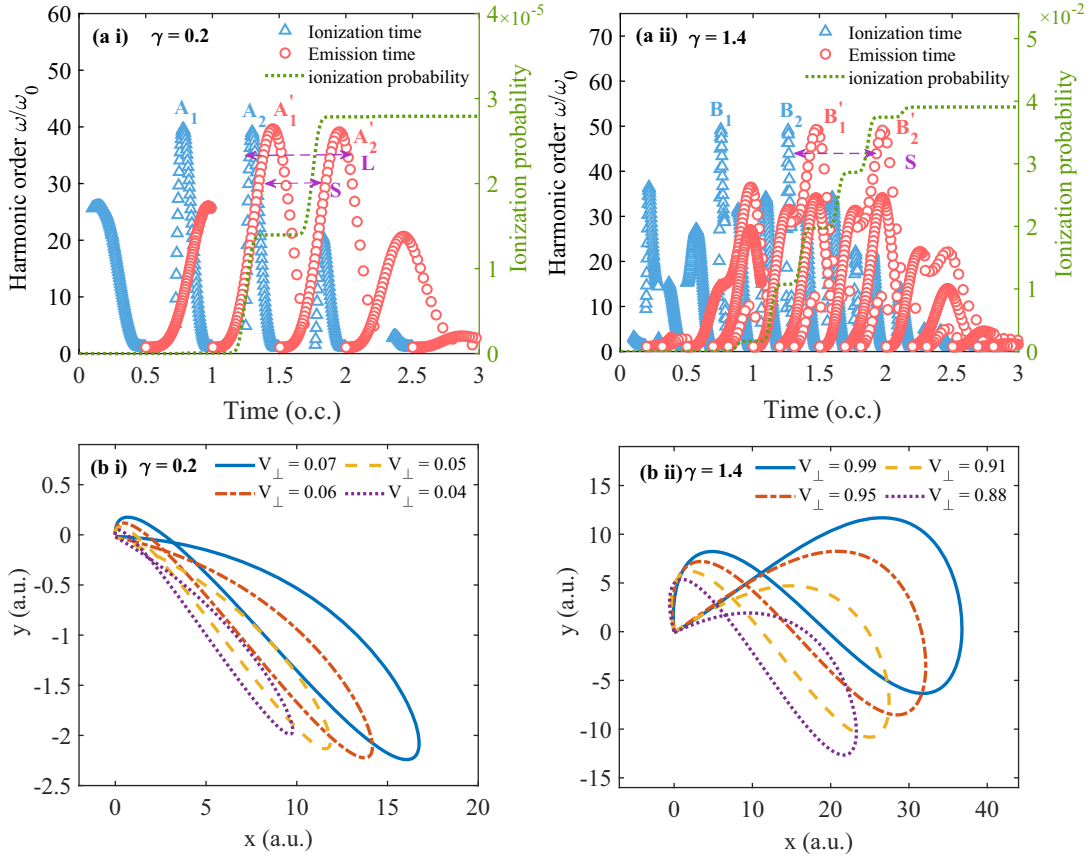


FIG. 5. Dependence of harmonic order on ionization (blue triangles) and emission time (red circles) and ionization probability (green dotted line) for the cases (a i) $\gamma = 0.2$ and (a ii) $\gamma = 1.4$ and electron trajectories for the cases (b i) $\gamma = 0.2$ and (b ii) $\gamma = 1.4$. The initial state is the $2p_+$ state and the other laser parameters are the same as those in Fig. 1.

means that the electron can be accelerated sufficiently to gain more energy. When the electron returns to the parent nucleus more energy will be released. Thus, the cutoff position of the harmonics has a certain extension as illustrated in Fig. 2(a) (red arrow) for $\gamma = 1.4$.

Next we use the trajectory of the electron and the maximum return kinetic energy of the electron to illustrate the physical mechanism of high-efficiency near-circularly-polarized HHG from the semiclassical three-step model [19,43]. The electron is located at the origin in the initial moment, and ignoring the Coulomb potential, the trajectory of the electron can be expressed as

$$\begin{aligned} x(t) &= \int_{t_0}^t \left(\int_{t_0}^{t'} E_x(t'') dt'' + v_{x0} \right) dt', \\ y(t) &= \int_{t_0}^t \left(\int_{t_0}^{t'} E_y(t'') dt'' + v_{y0} \right) dt', \end{aligned} \quad (8)$$

where t_0 is the ionization moment. The initial velocity components in the x and y directions can be written as

$$\begin{aligned} v_{x0} &= v_{\parallel} \cos(\theta_0) + v_{\perp} \sin(\theta_0), \\ v_{y0} &= -v_{\parallel} \sin(\theta_0) + v_{\perp} \cos(\theta_0), \end{aligned} \quad (9)$$

where $\theta_0 = \tan^{-1}[E_y(t_0)/E_x(t_0)]$ is the angle between the electric-field vector and the coordinate axis at the time t_0

and v_{\parallel} and v_{\perp} are the initial parallel velocity and transverse velocity, respectively [19]. The electrons are mostly ionized through tunneling; thus the initial velocity parallel to the ionization field is zero ($v_{\parallel} = 0$) [44]. By solving $x(t) = 0$ and $y(t) = 0$, the recombination time with proper finite initial velocity will be obtained and then we will get the trajectory and kinetic energy for the recombination time.

To better understand the physical mechanism of the harmonic emission, we show the dependence of the harmonic order on the ionization and emission time and the electron trajectories by the three-step model with nonzero initial velocity in Fig. 5 for the cases of $\gamma = 0.2$ and 1.4, respectively. We also show the ionization probability (green dotted line) for the cases of $\gamma = 0.2$ and 1.4 in Figs. 5(a i) and 5(a ii), respectively. The ionization probability is calculated from $P(t) = 1 - \exp[-\int_{-\infty}^t W(t') dt']$, where $W(t')$ is determined using the Ammosov-Delone-Krainov model [45].

From Fig. 5(a i) we can see that for the case of $\gamma = 0.2$ the harmonics near the cutoff position (30th to 40th order) are from the contribution of the two peaks A'_1 and A'_2 . The maximum return kinetic energy of the electron reaches about 40th order, which corresponds to the cutoff position of the harmonic for $\gamma = 0.2$, as shown in Fig. 2(a) (blue arrow). From the ionization probability as shown in Fig. 5(a i) we can see that the strongest contribution to the harmonics is from peak A'_2 and both long (L) and short (S) quantum

trajectories contribute to the harmonic emission, which indicates that there is strong interference between electron pathways and it is unfavorable to synthesize an isolated pulse. From Fig. 1(a iii) we can see that the pulse is not isolated for the case of $\gamma = 0.2$. The pulse train is obtained, with two intensity peaks (indicated by yellow arrows) in one cycle. From Fig. 5(a ii) we can see the harmonics near the cutoff position also from the contribution of the two peaks (B'_1 and B'_2) and the maximum return kinetic energy close to the 50th order, which is in agreement with that shown in Fig. 2(a) (red arrow). Similarly, we can see that the strongest contribution to the harmonics is from peak B'_2 based on the ionization probability. The difference is that the contribution is mainly from the short (S) quantum trajectory of peak B'_2 with weaker interelectron interference, which is thus beneficial to synthesize the isolated radiation pulse [see Fig. 3(b i)]. Moreover, by comparing the ionization probability for the cases of $\gamma = 0.2$ and 1.4, the ionization probability in the case of $\gamma = 1.4$ is three orders of magnitude higher than that in the case of $\gamma = 0.2$, which results in the enhancement of the harmonics.

In Figs. 5(b i) and 5(b ii) we show the electron trajectories for the cases of $\gamma = 0.2$ and 1.4, respectively. The electrons have nonzero transverse initial velocity due to the transverse velocity distribution of the electron wave packet at the exit of the tunnel during the HHG processes [44]. Classical electron trajectories are obtained for electron ionization from $T = 1.25$ to 1.4 o.c. These electrons are recombined with the parent nucleus around $T = 1.9$ o.c., as shown in Figs. 4(a v) and 4(b v), and correspond to the peaks A'_2 and B'_2 as shown in Figs. 5(a i) and 5(a ii).

In Ref. [33] the authors indicate that the ring-current state carries angular momentum, which breaks the symmetry of the system and the angular momentum deflects the ionized electrons away from the x axis, so the intensity of the y component of the harmonics is not zero. It is also shown that the harmonics from ring-current state driven by the OTC laser fields will have larger ellipticity due to the fact that the electrons have a helical trajectory; thus the intensity of the y component of the harmonics is enhanced. From Fig. 5(b i) we can see that for the case of $\gamma = 0.2$ the electron moves about 2 a.u. on the y axis and about 17 a.u. on the x axis, which indicates that the electron motion has a small helical trajectory and moves mainly along the x axis. From Fig. 5(b ii) we can see that for the case of $\gamma = 1.4$, the electron moves about 16 a.u. on the y axis and about 35 a.u. on the x axis. The electrons move with a larger helical trajectory and move farther in the y axis direction, which enhances the intensity of the y component of the harmonics. It makes the harmonic intensity of the x and y components closer to each other, which causes the ellipticity of the harmonics to be larger [42]. Our result is consistent with that described in Ref. [33]. Moreover, the electrons move farther and can be effectively accelerated by the laser field, which will obtain larger energy and thus the cutoff position of the harmonics has a certain extension. The above results are consistent with the analysis of the quantum perspective as illustrated in Fig. 4.

As we know, the relative phase of the OTC laser fields also has an important effect on the harmonics [46–48]. For example, by adjusting the relative phase of the laser field, the contribution of long and short quantum trajectories to

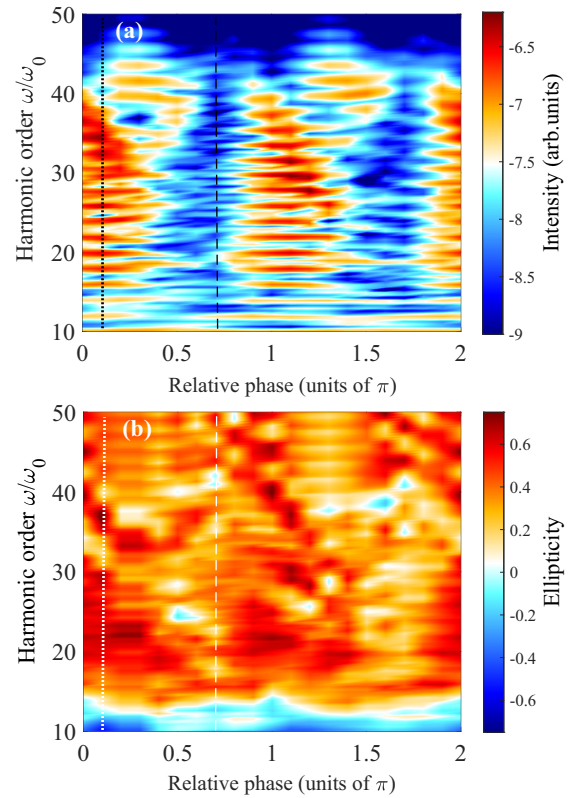


FIG. 6. (a) Intensity and (b) ellipticity distribution of the harmonics versus harmonic order and relative phase ϕ . The intensity ratio of the OTC fields is $\gamma = 1.4$. The initial state is the $2p_+$ state and the other laser parameters are the same as those in Fig. 1. The harmonic intensity is on a logarithmic scale.

the harmonics can be controlled [46]. We investigate the effect of the relative phase of the OTC fields on the harmonic intensity and ellipticity for the case of $\gamma = 1.4$ as shown in Fig. 6.

Figure 6(a) shows the dependence of the harmonic intensity distribution on relative phase and harmonic order, which can be seen in the harmonic intensity being sensitive to the variation of relative phase. For example, the harmonic intensity has a maximum around 0.1π (black dotted line) and a minimum around 0.7π (black dashed line). Habibović *et al.* [48] investigated the variation of the harmonic intensity of the CO_2 molecule with relative phase and harmonic order based on the OTC fields as shown in Fig. 2 (top left) of Ref. [48]. We can see that the intensity of the harmonics is sensitive to the relative phase variation. For example, Fig. 2 (top left) of Ref. [48] showed that around 18° (0.1π) the harmonic intensity is stronger, while around 126° (0.7π) the harmonic intensity is weaker. Our result is similar to that illustrated in Ref. [48].

Figure 6(b) shows the dependence of the ellipticity of the harmonics on the relative phase and harmonic order. From Fig. 6(b) we can see that the ellipticity of the harmonics is also sensitive to the relative phase. For example, the ellipticity of harmonics is higher around 0.1π (white dotted line) and lower around 0.7π (white dashed line). The distribution of harmonic ellipticity and intensity is similar as the relative

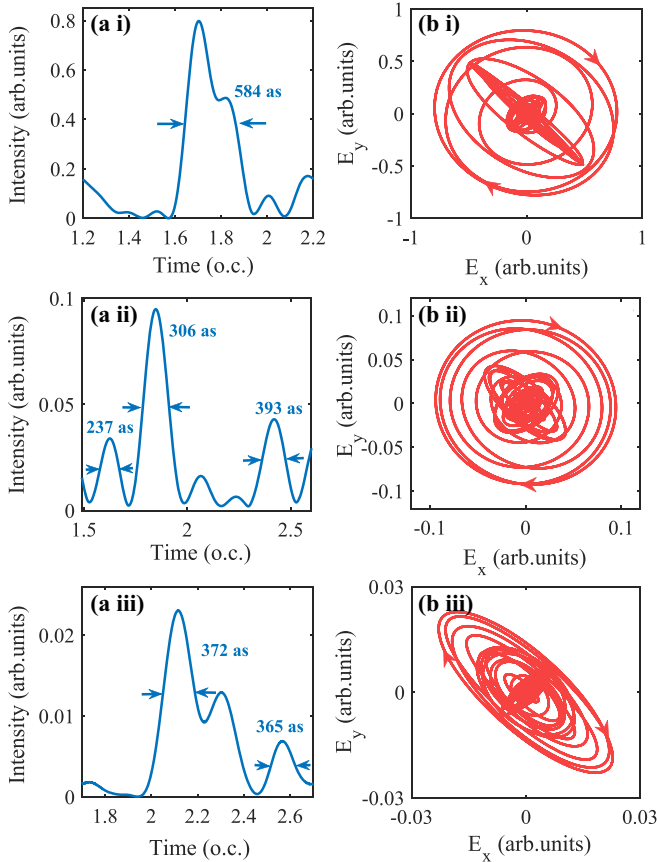


FIG. 7. Time-dependent intensity of the single-atom radiation pulse synthesized by the harmonic spectrum in the range from the 29th to the 36th order for the case of (a i) $\phi = 0.1\pi$ and from the 35th to the 40th order for the cases of (a ii) $\phi = 0.2\pi$ and (a iii) $\phi = 0.7\pi$. Also shown is the electric-field projection of the radiation pulse on the E_x - E_y cases of (b i) $\phi = 0.1\pi$ and $\epsilon = 0.95$, (b ii) $\phi = 0.2\pi$ and $\epsilon = 0.93$, and (b iii) $\phi = 0.7\pi$ and $\epsilon = 0.41$. The intensity ratio of OTC fields is $\gamma = 1.4$. The initial state is the $2p_+$ state and the other laser parameters are the same as those in Fig. 1.

phase ϕ changes. Moreover, we can see that the ellipticity of the harmonics in the plateau region (20th to 50th order) is almost positive, i.e., the harmonics are right elliptically polarized. Sun *et al.* [49] also investigated the variation of the ellipticity distribution of the CO molecule as a function of relative phase and harmonic order in the OTC fields [see Fig. 1(a) of Ref. [49]]. The difference is that the harmonic helicity appears alternately: Around 0.1π the ellipticity of the harmonic is negative (left elliptical polarization) and around 0.7π the ellipticity of the harmonic is positive (right elliptical polarization). The reason is that in our result the initial state is the ring-current state $2p_+$ and the polarization characteristics of the harmonics depend on the initial orbit rather than on the driving field [29,33]. Therefore, in our result the helicity of the harmonics is always the same whether the intensity ratio or the relative phase of the OTC fields is changed.

In Fig. 7 we present the time-dependent intensity of the single-atom radiation pulse and the projection of the electric field of the single-atom radiation pulse onto the E_x - E_y plane through the superposition of the harmonic spectrum near the cutoff position for the intensity ratio $\gamma = 1.4$. Figure 7(a i) shows the time-dependent intensity of the radiation pulse by superimposing 29th- to 36th-order harmonics for the case of $\phi = 0.1\pi$, and we can see that the radiation pulse with a duration of 584 as can be obtained. Figure 7(b i) shows the projection of the electric field of the radiation pulse onto the E_x - E_y plane for $\phi = 0.1\pi$. We can see that the ellipticity of the radiation pulse is 0.95 and is right-rotating polarized (red arrow). Figures 7(a ii) and 7(a iii) show the time-dependent intensity of the radiation pulse by superimposing 35th- to 40th-order harmonics for the cases of $\phi = 0.2\pi$ and 0.7π . We find that the radiation is a pulse train and the highest intensity pulse has a duration of 306 as for $\phi = 0.2\pi$ and 372 as for $\phi = 0.7\pi$. In Figs. 7(b ii) and 7(b iii) we show the projection of the electric field of the radiation pulse onto the E_x - E_y plane. We can see that the ellipticity of the radiation pulse is 0.93 for $\phi = 0.2\pi$ and 0.41 for $\phi = 0.7\pi$ and the pulses are right-rotating polarized (red arrow). The above results show that near-circularly-polarized single-atom radiation pulse can be obtained for $\phi = 0.1\pi$ and 0.2π and the elliptically polarized radiation pulse for $\phi = 0.7\pi$. Therefore, the above analysis illustrates that the ellipticity of the single-atom radiation pulse is very sensitive to the relative phase. By varying the relative phase of the OTC laser fields, it is possible to control the polarization and temporal profile of the single-atom radiation pulse in the temporal domain.

IV. CONCLUSION

In summary, we have demonstrated a scheme to generate a near-circularly-polarized pulse from single-atom radiation with high efficiency. It is based on the ring-current state of the Ne atom in OTC fields. The ellipticity of harmonics originates from the ring-current state with nonzero angular momentum. The intensity and ellipticity of the harmonics increase as the OTC intensity ratio increases. By adjusting the intensity ratio of the OTC laser fields, a near-circularly-polarized single-atom radiation pulse with high efficiency can be obtained at specific intensity ratios. It can be interpreted by analyzing the time evolution of the probability density of the electron wave packet and the semiclassical three-step model. Moreover, the intensity and ellipticity of the harmonics are very sensitive to the relative phase of the OTC laser fields. The polarization and the temporal profile of the radiation pulse in the time domain can be controlled. Our results provide a method for generating a near-circularly-polarized single-atom radiation pulse with high efficiency. The scheme is expected to provide a useful light source for the molecular chiral recognition and differential measurements of circular dichroism.

ACKNOWLEDGMENTS

This work was supported by the National Natural Science Foundation of China (Grants No. 12074142 and No. 12374265).

- [1] P. B. Corkum, *Phys. Rev. Lett.* **71**, 1994 (1993).
- [2] R. Kienberger, M. Hentschel, M. Uiberacker, C. Spielmann, M. Kitzler, A. Scrinzi, M. Wieland, T. Westerwalbesloh, U. Kleineberg, U. Heinzmann, M. Drescher, and F. Krausz, *Science* **297**, 1144 (2002).
- [3] E. Goulielmakis, Z. H. Loh, A. Wirth, R. Santra, N. Rohringer, V. S. Yakovlev, S. Zherebtsov, T. Pfeifer, A. M. Azzeer, M. F. Kling, S. R. Leone, and F. Krausz, *Nature (London)* **466**, 739 (2010).
- [4] D. Azoury, O. Kneller, S. Rozen, B. D. Bruner, A. Clergerie, Y. Mairesse, B. Fabre, B. Pons, N. Dudovich, and M. Krüger, *Nat. Photon.* **13**, 54 (2019).
- [5] S. Baker, J. S. Robinson, C. A. Haworth, H. Teng, R. A. Smith, C. C. Chirilă, M. Lein, J. W. G. Tisch, and J. P. Marangos, *Science* **312**, 424 (2006).
- [6] H. Niikura, N. Dudovich, D. M. Villeneuve, and P. B. Corkum, *Phys. Rev. Lett.* **105**, 053003 (2010).
- [7] S. Ghimire, A. D. DiChiara, E. Sistrunk, P. Agostini, L. F. DiMauro, and D. A. Reis, *Nat. Phys.* **7**, 138 (2011).
- [8] G. Vampa, T. J. Hammond, N. Thiré, B. E. Schmidt, F. Légaré, C. R. McDonald, T. Brabec, and P. B. Corkum, *Nature (London)* **522**, 462 (2015).
- [9] L. Li, P. Lan, X. Zhu, T. Huang, Q. Zhang, M. Lein, and P. Lu, *Phys. Rev. Lett.* **122**, 193901 (2019).
- [10] J. Li, X. Ren, Y. Yin, K. Zhao, A. Chew, Y. Cheng, E. Cunningham, Y. Wang, S. Hu, Y. Wu, M. Chini, and Z. Chang, *Nat. Commun.* **8**, 186 (2017).
- [11] T. Gaumnitz, A. Jain, Y. Pertot, M. Huppert, I. Jordan, F. Ardana-Lamas, and H. J. Wörner, *Opt. Express* **25**, 27506 (2017).
- [12] A. Ferré, C. Handschin, M. Dumergue, F. Burgy, A. Comby, D. Descamps, B. Fabre, G. A. Garcia, R. Géneaux, L. Merceron, E. Mével, L. Nahon, S. Petit, B. Pons, D. Staedter, S. Weber, T. Ruchon, V. Blanchet, and Y. Mairesse, *Nat. Photon.* **9**, 93 (2015).
- [13] D. Ayuso, P. Decleva, S. Patchkovskii, and O. Smirnova, *J. Phys. B* **51**, 06LT01 (2018).
- [14] N. Böwering, T. Lischke, B. Schmidtke, N. Müller, T. Khalil, and U. Heinzmann, *Phys. Rev. Lett.* **86**, 1187 (2001).
- [15] O. Travnikova, J. C. Liu, A. Lindblad, C. Nicolas, J. Söderström, V. Kimberg, F. Gel'mukhanov, and C. Miron, *Phys. Rev. Lett.* **105**, 233001 (2010).
- [16] O. Kfir, P. Grychtol, E. Turgut, R. Knut, D. Zusin, D. Popmintchev, T. Popmintchev, H. Nembach, J. M. Shaw, A. Fleischer, H. Kapteyn, M. Murnane, and O. Cohen, *Nat. Photon.* **9**, 99 (2015).
- [17] D. D. Hickstein, F. J. Dollar, P. Grychtol, J. L. Ellis, R. Knut, C. Hernández-García, D. Zusin, C. Gentry, J. M. Shaw, T. Fan, K. M. Dorney, A. Becker, A. Jaroń-Becker, H. C. Kapteyn, M. M. Murnane, and C. G. Durfee, *Nat. Photon.* **9**, 743 (2015).
- [18] K. S. Budil, P. Salières, A. L'Huillier, T. Ditmire, and M. D. Perry, *Phys. Rev. A* **48**, R3437 (1993).
- [19] M. Möller, Y. Cheng, S. D. Khan, B. Zhao, K. Zhao, M. Chini, G. G. Paulus, and Z. Chang, *Phys. Rev. A* **86**, 011401(R) (2012).
- [20] X. Zhou, R. Lock, N. Wagner, W. Li, H. C. Kapteyn, and M. M. Murnane, *Phys. Rev. Lett.* **102**, 073902 (2009).
- [21] A.-T. Le, R. R. Lucchese, and C. D. Lin, *Phys. Rev. A* **82**, 023814 (2010).
- [22] Y.-H. Xing, J. Zhang, X.-X. Huo, Q.-Y. Xu, and X.-S. Liu, *Chin. Phys. B* **31**, 043203 (2022).
- [23] K. M. Dorney, J. L. Ellis, C. Hernández-García, D. D. Hickstein, C. A. Mancuso, N. Brooks, T. Fan, G. Fan, D. Zusin, C. Gentry, P. Grychtol, H. C. Kapteyn, and M. M. Murnane, *Phys. Rev. Lett.* **119**, 063201 (2017).
- [24] D. B. Milošević, *Opt. Lett.* **40**, 2381 (2015).
- [25] X. Liu, X. Zhu, L. Li, Y. Li, Q. Zhang, P. Lan, and P. Lu, *Phys. Rev. A* **94**, 033410 (2016).
- [26] K. J. Yuan, S. Chelkowski, and A. D. Bandrauk, *J. Phys. Chem. A* **125**, 7111 (2021).
- [27] P.-C. Huang, C. Hernández-García, J.-T. Huang, P.-Y. Huang, C.-H. Lu, L. Rego, D. D. Hickstein, J. L. Ellis, A. Jaron-Becker, A. Becker, S.-D. Yang, C. G. Durfee, L. Plaja, H. C. Kapteyn, M. M. Murnane, A. H. Kung, and M.-C. Chen, *Nat. Photon.* **12**, 349 (2018).
- [28] S. Gamsheim and J.-M. Rost, *Phys. Rev. A* **100**, 043408 (2019).
- [29] X. Zhang, X. Zhu, X. Liu, F. Wang, M. Qin, Q. Liao, and P. Lu, *Phys. Rev. A* **102**, 033103 (2020).
- [30] X. Xie, A. Scrinzi, M. Wickenhauser, A. Baltuška, I. Barth, and M. Kitzler, *Phys. Rev. Lett.* **101**, 033901 (2008).
- [31] D. Wang, X. Zhu, H. Yuan, P. Lan, and P. Lu, *Phys. Rev. A* **101**, 023406 (2020).
- [32] M. B. Gaarde, J. L. Tate, and K. J. Schafer, *J. Phys. B* **41**, 132001 (2008).
- [33] O. Neufeld and O. Cohen, *Phys. Rev. Lett.* **123**, 103202 (2019).
- [34] I. Barth and J. Manz, *Phys. Rev. A* **75**, 012510 (2007).
- [35] S. Eckart, M. Kunitski, M. Richter, A. Hartung, J. Rist, F. Trinter, K. Fehre, N. Schlott, K. Henrichs, L. P. H. Schmidt, T. Jahnke, M. Schöffler, K. Liu, I. Barth, J. Kaushal, F. Morales, M. Ivanov, O. Smirnova, and R. Dörner, *Nat. Phys.* **14**, 701 (2018).
- [36] I. Barth, J. Manz, Y. Shigeta, and K. Yagi, *J. Am. Chem. Soc.* **128**, 7043 (2006).
- [37] X. Zhang, L. Li, X. Zhu, K. Liu, X. Liu, D. Wang, P. Lan, I. Barth, and P. Lu, *Phys. Rev. A* **98**, 023418 (2018).
- [38] I. Barth and M. Lein, *J. Phys. B* **47**, 204016 (2014).
- [39] L. Medišauskas, J. Wragg, H. van der Hart, and M. Y. Ivanov, *Phys. Rev. Lett.* **115**, 153001 (2015).
- [40] X. Zhang, X. Zhu, X. Liu, D. Wang, Q. Zhang, P. Lan, and P. Lu, *Opt. Lett.* **42**, 1027 (2017).
- [41] J. Zhang, S. Wang, X.-X. Huo, Y.-H. Xing, F. Wang, and X.-S. Liu, *Opt. Commun.* **530**, 129152 (2023).
- [42] S.-K. Son, D. A. Telnov, and S.-I. Chu, *Phys. Rev. A* **82**, 043829 (2010).
- [43] C.-L. Xia and X.-S. Liu, *Phys. Rev. A* **87**, 043406 (2013).
- [44] X. L. Ge, H. Du, J. Guo, and X. S. Liu, *Opt. Express* **23**, 8837 (2015).
- [45] M. V. Ammosov, N. B. Delone, and V. P. Kraïnov, *Sov. Phys. JETP* **64**, 1191 (1986).
- [46] L. Brugnera, D. J. Hoffmann, T. Siegel, F. Frank, A. Zaïr, J. W. G. Tisch, and J. P. Marangos, *Phys. Rev. Lett.* **107**, 153902 (2011).
- [47] I. J. Kim, C. M. Kim, H. T. Kim, G. H. Lee, Y. S. Lee, J. Y. Park, D. J. Cho, and C. H. Nam, *Phys. Rev. Lett.* **94**, 243901 (2005).
- [48] D. Habibović, W. Becker, and D. B. Milošević, *J. Phys. B* **54**, 134004 (2021).
- [49] N. Sun, Y. T. Chen, Y. H. Chen, and X. S. Zhu, *J. Phys. B* **55**, 205602 (2022).